# Bidirectional Marx DC-DC Converter for Offshore Wind Farm Application

## S M Alagab, S B Tennakoon, C A Gould

*School of Creative Arts and Engineering, Staffordshire University, Stoke on Trent, United Kingdom*
*samir.alagab@research.staffs.ac.uk, S.B.Tennakoon@staffs.ac.uk, C.A.Gould@staffs.ac.uk*

## Abstract

The bidirectional DC-DC converter explained in this paper is based on the Marx principle, and is capable of achieving step-up and step-down voltage transformations at kV level and is able to handle MW level power transfers in both directions. The main features of this topology is the absence of a high-frequency transformer, reduced weight, volume, and soft switching to reduce the switching losses. In the boost mode, five capacitors are charged in parallel and discharged in series to achieve the step-up action, and in the buck mode the converse action takes place. The operating principle is explained, and the steady-state analysis of the converter is given. Matlab/Simulink simulation of a 50MW converter, interfacing 6kV, and 30kV systems supports and the validates the theoretical analysis, enables positive supporting the conclusions to be made.

## 1 Introduction

A High Voltage Direct Current (HVDC) grid is a natural extension of the grid integration of large offshore wind farms using Voltage Source Converter (VSC) based HVDC Systems. Such systems would require the interconnection of sections operating at different DC voltage levels through DC-DC converters [1]. The power flow through the DC-DC converter needs to be in both directions. During normal generation, the power flow is from the wind farm to the grid. However, when the wind farm is not generating, the auxiliaries in the wind farm require a small amount of power which must be drawn from the grid. Therefore, the DC-DC converter needs to be bidirectional.

This paper is organised as follows: in section 2 a number of bidirectional DC-DC converter topologies found in literature are explained. A new bidirectional converter and its steady-state analysis is presented in Sections 3 and 4, respectively. In section 5, a simulation study in the forward and reverse mode has been presented. Finally, conclusions are drawn in section 6.

## 2 Bidirectional DC-DC converter topologies

Dual Active Bridge (DAB) converter [2],[3],[4], [5] shown in Fig. 1(a), typically operates at a high switching frequency in order to reduce the size of the transformer. Although these topologies use soft switching to reduce switching losses, their magnetic core losses are still high and have high ripple currents and large leakage inductances. These converters also require complex control.

Thomas [5], has presented three types of DAB converter, which require complex control. Xing [6] presented a modular bidirectional buck/boost DC/DC converter for HVDC grid as illustrated in Figure 1(b). It uses small submodule capacitors when compared to the modular multilevel converter, which will significantly reduce the converter volume and weight, but the drawback of this converter is the variable duty cycle and large inductance.

In Figure 1(c), Pires [7] presented a bi-directional buck/boost converter for electrochemical storage devices. The voltage ratio of this converter is high but has a variable duty cycle in both forward and reverse operation. The switching frequency is high, leading to high switching losses and hence is impractical in high power converters.

Dragan [8] proposed a high power DC converter without a transformer which uses thyristors as switching devices as shown in Figure 1(d). It can transfer the power in both directions and has an ability to isolate faults. However, the Dragan's converter has 8 inductors and requires several switches in series to withstand the high voltage.

LCL bidirectional DC-DC converter [9],[10] shown in Figure 1(e), uses IGBTs unlike the Dragan converter [8]. The advantage of this converter is the ability to achieve current regulation, even under extreme external DC faults and soft switching to reduce the switching losses. The disadvantage of this converter is the large size of inductor requires to reduce the current ripple and requires series connection of devices. In addition, Kolparambath presented an LCL bidirectional DC-DC converter in multiterminal direct current MTDC systems [11] as depicted in Figure 1(f). This converter has one inductor which is an advantage, high voltage ratio and a low switching frequency. However, the inductor is large and requires many switches in series to withstand the high voltage. This converter uses hard switching, which leads to high switching losses.

Filsoof [12] developed a bidirectional modular multilevel DC-DC converter of the triangular structure as illustrated in Figure 1(g). This converter has a significant reduction in the output voltage ripple and input current. However, this topology suffers` from high switching frequency and has a

two-level structure with only one boost inductor. This leads to design difficulties for HVDC application.



a)



b)                              c)



d)



e)
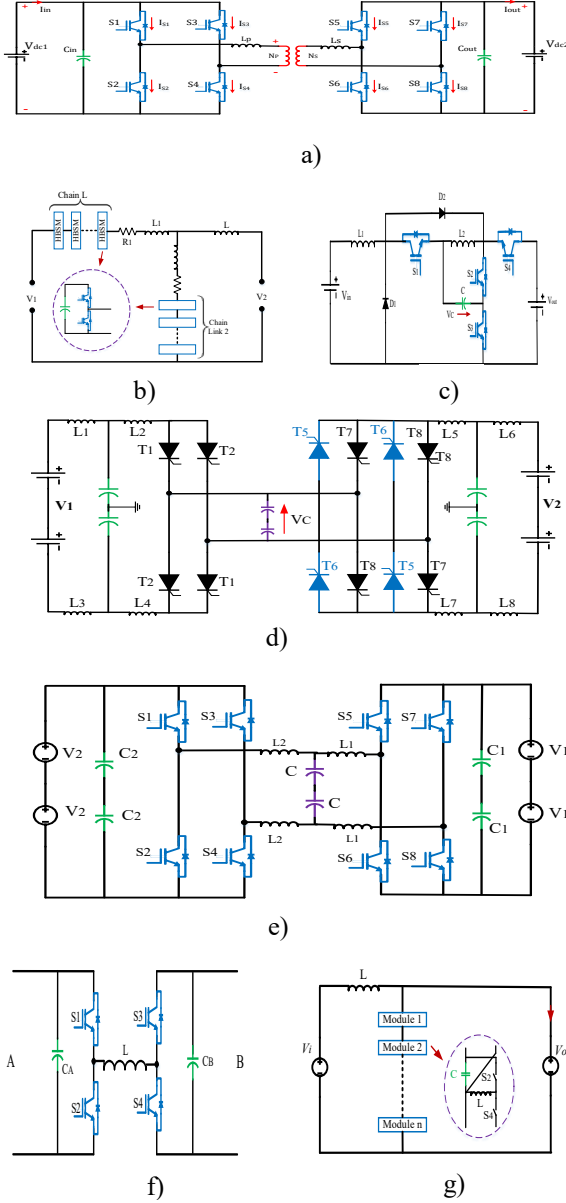


f)                              g)

Figure 1: Common bidirectional DC-DC converter topologies: (a) DAB, (b) Modular buck/boost, (c) buck/boost quadratic, (d) Thyristor converter, (e) IGBT converter (f) Four quadrant converter, and g) MMC converter.

# 3 Bidirectional DC-DC Marx converter

## 3.1 Circuit Configuration

The main circuit of the bidirectional DC-DC Marx converter is illustrated in Figure 3. It consists of three circuits. The first circuit is comprised of inductor $L_1$ and capacitor $C_L$ connected in series with DC voltage $V_L$.

There are five identical modules in the second circuit. Each module is composed of three cells A, B, and C; cells A and C have two anti-parallel IGBT switches with diodes connected in series and a capacitor for holding the cell voltage. Cell B has two anti-parallel IGBT switches only. The converter can transfer the power in both directions and scale the voltage up or down the transformation ratio by changing the number of modules. The third circuit is similar to the first consisting of the inductor $L_2$ and the capacitor $C_H$ connected in series with the DC voltage $V_H$

## 3.2 The operating principle

The operation of the converter is based on the Marx generator concept. Five modules are used to achieve a voltage ratio of 1:5. In this study, a range of power levels up to 50MW in the forward direction and up to 5MW in reverse direction are considered.

All the IGBTs are switched at zero current to reduce the switching losses. In addition, all the switches must be capable of bidirectional blocking and forward conducting. The converter operation can be divided into two modes of operation; Forward Mode (FM) and reverse mode (RM).

- ### Forward Mode

In this mode, the energy flows from the low voltage side to the high voltage side. Forward-mode can also be divided into two sub-commutations. In the first sub-commutation ($t_0$-$t_1$) as shown in Figure 2, the charging current flows through five capacitors ($C_1$-$C_5$) in parallel by switching ON switches ($S_A$-$S_B$), while all the other switches are turned OFF, as shown in Figure 4. The diodes ($D_A$) block the reverse current flow.

In the second sub-commutation ($t_1$-$t_2$) the capacitors that were charged during the first sub-commutation are discharged in series to create the high voltage on the HV side by switching ON switches ($S_C$), while diodes ($D_C$) block the reverse current flow during capacitor discharge.

In this case, as there are 5 modules the voltage gain is 5 and the electric charges is transferred from the five series-connected capacitors $C_1$, $C_2$, $C_3$, $C_4$ and $C_5$ to the capacitor $C_H$ as depicted in Figure 5.
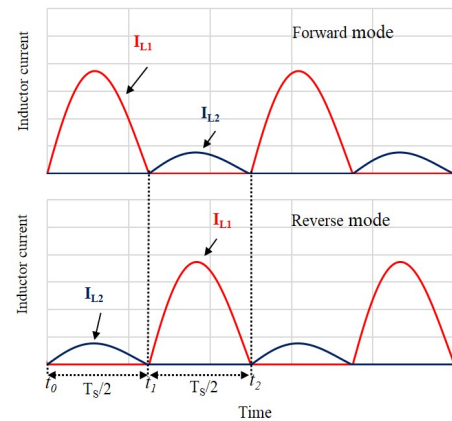


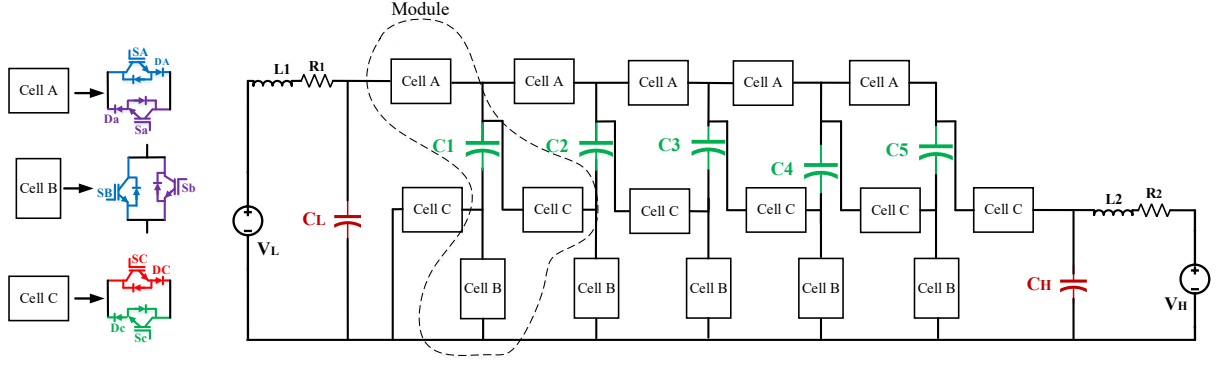Figure 2: Inductor current waveforms during both modes
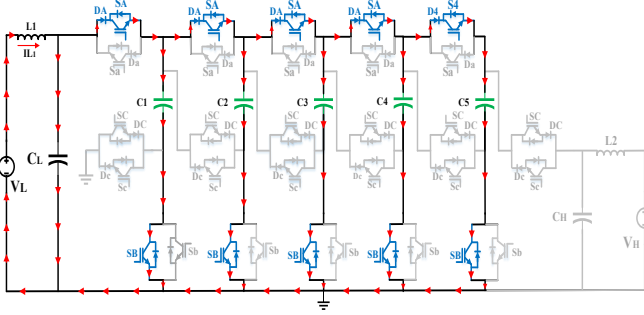
Figure 3: Bidirectional DC-DC converter



Figure 4: Switching and corresponding current flow directions of charging capacitors in parallel in forward mode
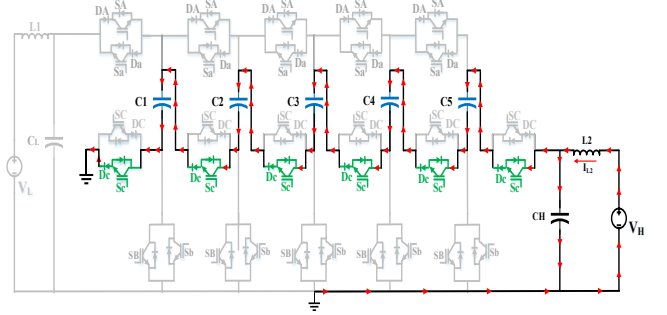


Figure 6: Switching and corresponding current flow direction of charging capacitors in series in reverse mode
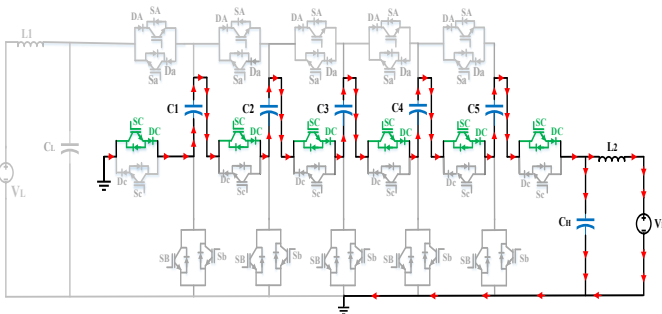


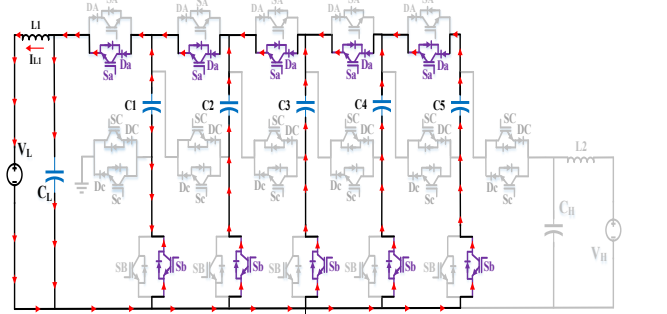Figure 5: Switching and corresponding current flow directions of discharging capacitors in series in FM



Figure 7: Discharging capacitors in parallel in reverse mode

- **Reverse Mode**

As shown in Figure 6, the current flows from high voltage $V_H$ to the low voltage $V_L$. In the first sub-commutation, inductor current $I_{L2}$ charges the five capacitors ($C_1$-$C_5$) in series in time interval ($t_0$-$t_1$), as shown in Figure 2, by switching ON switches ($S_C$) and diodes ($D_C$), are connected in series with switches ($S_C$) to ensure unidirectional transfer of charge from the voltage source $V_H$, to series-connected capacitors and which are forward biased, while all the other switches are turned OFF.

In the second sub-commutation, the switches ($S_a$, $S_b$) are turned ON, and the capacitors are discharged in parallel in time interval ($t_1$-$t_2$) to the low voltage $V_L$ through inductor $L_1$

as depicted in Figure 2, while the other switches are turned OFF as shown in Figure 7.

## 4   Steady-state analysis

It is assumed that the converter has reached the steady-state condition. The converter voltage gain is the same as the number of capacitors "n" and hence;

$$n = \frac{V_H}{V_L} \qquad (1)$$

where $V_L$ and $V_H$ are the low side and high side voltages, respectively. The equivalent capacitance in forward mode at the first sub-commutation is

$$C_{eq} = \sum_{k=1}^{k} C_i \qquad (2)$$

where $C_i$ is the capacitance, and $C_{eq}$ is the equivalent capacitance of parallel connected capacitors in the first sub-commutation. However, in the first-commutation, the inductor $L_1$ and the equivalent capacitance $C_{eq\,(J)}$ forms an oscillatory L-C circuit and hence the current in the first sub-commutation is given by,

$$i_{L1} = i_{Ceq} = \frac{V_L}{\omega L_1} \sin(\omega t) \qquad (3)$$

and

$$\omega = \frac{1}{\sqrt{L_1 C_{eq}}} \qquad (4)$$

Based on the designed power rating of the bidirectional converter and the charge transfer, the inductor $L_1$ can be given as;

$$L_1 = \frac{1}{C_{eq}} \left[ \frac{Q\, n V_L}{2\pi\, P_{rate}} \right]^2 \qquad (5)$$

Where $P_{rate}$ is the rating power of the converter and $Q$ is the amount of charge during charging in parallel. The value of inductor $L_2$ depends on the peak-to-peak of output current $\Delta I_{L2}$ and can be expressed as;

$$L_2 = \left[ \frac{n V_L\, T_S}{\Delta I_{L2}} \right]^2 \qquad (6)$$

The determination of the capacitance value $C_{eq}$, is based on the capacitor voltage ripple and the amount of charge in the cycle.

$$C_{eq} = \frac{Q}{\Delta VC} \qquad (7)$$

The value of high side voltage capacitor $C_H$ depends on the relationship between the amount of charge to output converter voltage $V_2$ at the half period ($T_S/2$) and the voltage ripple on the capacitor $C_H$. Hence,

$$C_H = \frac{\left( P_{rate} / V_2 \right) \left( T_S / 2 \right)}{2\pi\, \Delta VC_H} \qquad (8)$$

Similarly, the value of low side voltage capacitor $C_L$ can be expressed as;

$$C_L = \frac{\left( P_{rate} / V_1 \right) \left( T_S / 2 \right)}{2\pi\, \Delta VC_L} \qquad (9)$$

## 5   Simulation Studies

The location of the converter studied in this paper is shown within the blue star in Figure  9. The total power is 50MW and the voltages are 6kV and 30kV. The windfarms cluster is formed by two parallel lines of wind turbines, each containing 5 wind turbines in series. Hence, there is a total of

10 wind turbines; each rated at 5 MW, 1.2 kV [13], [14],[15]. The DC-DC Converter is required to transfer the power in both directions, and is connected to the collection bus tie interconnect at the 6kV side to the 30kV side. The forward and reverse powers are 50MW and 5MW. Using the equations derived in section 4, the parameters of the DC-DC converter used for the simulation were calculated and are listed in Table 1.
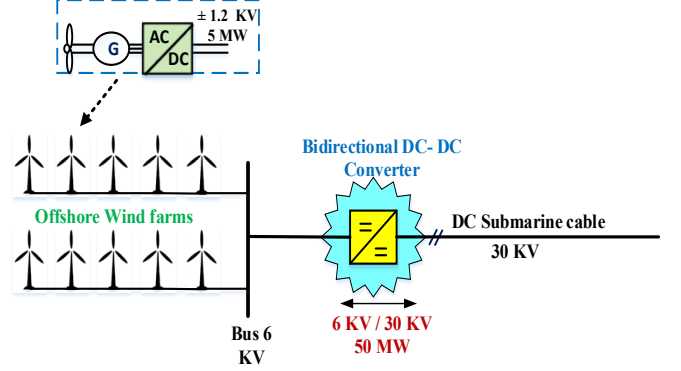


Figure   8: DC collection topology system of wind farm

As the interest is on the converter operation, the system shown in Figure 8 was reduced to the circuit shown in Figure 9. The two systems on either side of the converter are represented by two voltage sources behind equivalent resistances and inductances. In practice, the power flow is controlled by the VSC at the onshore substation. However, for the simulation, the power flow was controlled by varying the resistance values $R_1$ and $R_2$ on both sides.
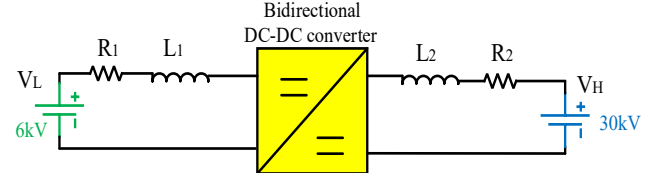


Figure   9: Simulation circuit diagram

| Parameters | | value | |
|---|---|---|---|
| Number of modules | | 5 | |
| Low Voltage | $V_L$ | 6 | kV |
| High Voltage | $V_H$ | 30 | kV |
| Inductor | $L_1$ | 2.53 | µH |
| Inductor | $L_2$ | 110 | µH |
| Capacitor in the middle circuit | $C_n$ | 694.5 | µF |
| Capacitor | $C_L$ | 83 | µF |
| Capacitor | $C_H$ | 116 | µF |
| Rated power | $P_{rate}$ | +50, -5 | MW |
| Frequency | $F_S$ | 2 | kHz |

Table 1: Converter Parameters used for circuit simulation

The switching frequency $F_S$ of the converter is determined by the LC resonances in the circuit and is 2 kHz, and the fixed duty cycle of $d$=50% was used. The converter is simulated in

Matlab/Simulink, using the SimPowerSystem toolbox. The waveforms of the voltage, current, and power during forward mode is depicted in Figure 10.

The DC gain obtained by the simulation is 4.9, which is very close to the design value of 5. The output voltage, current, and power of the converter in forward mode operation should be 30 KV/ 1667A, 50MW as designed. However, the output voltage of the proposed converter is 29.97KV and the current is 1659A. In addition, the load power is 49.7MW as shown in Figure 10.

During discharging the capacitors in series, the voltage across the IGBT switches SC is 6 kV as shown in Figure 11c. However, the voltages across switches $S_B$ increases by 6kV from left to right reaching a maximum of 24kV on the shunt IGBT switch at the HV side as shown in Figure 11(d). This means that the devices in each module sees different voltages causing manufacturing issues and requiring series connection of devices. In addition, a reverse voltage of 6kV appears across switches SA as illustrated in Figure 11(e).
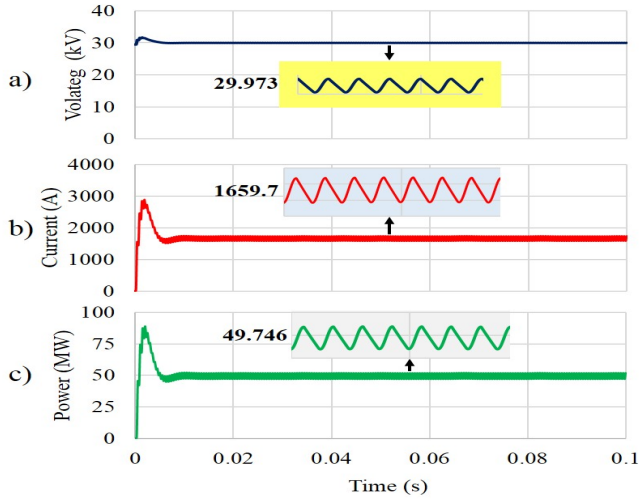


Figure 10: Simulation waveforms of the forward mode operation

As illustrated in Figure 11(a) and Figure 11(b), IGBT and Diode currents in modules 1,2,3,4,5 increases, peaking at 18.6 kA in 250 µs in the last module. IGBTs capable of this duty are commercially available. An example is the IGBT 5SNA 1200G450300 [16].
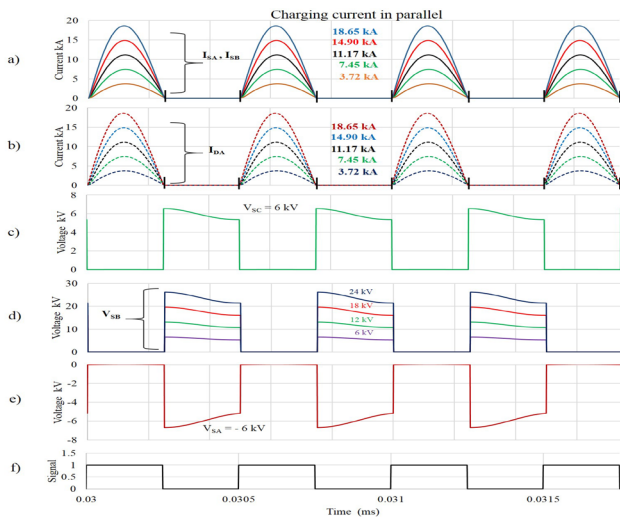


Figure 11: IGBT and diode switch simulation waveforms of forward mode operation: (a) charging current through IGBTs, (b) charging current through diodes, (c) voltage across cells C, (d) voltage across cells B, (e) voltage across cells A, and (f) switching pattern.
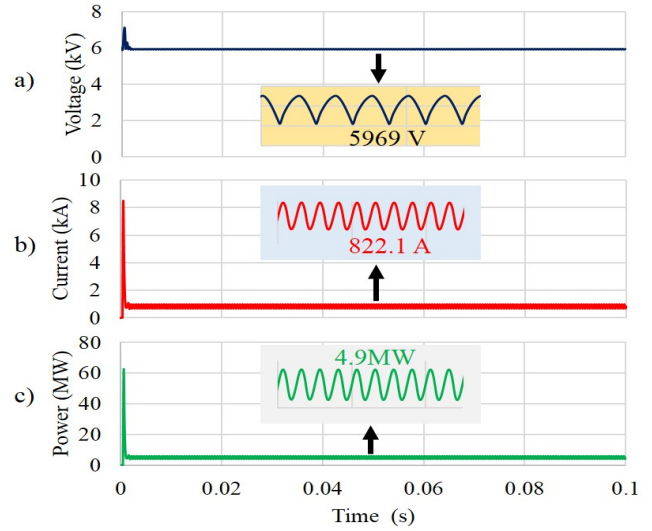


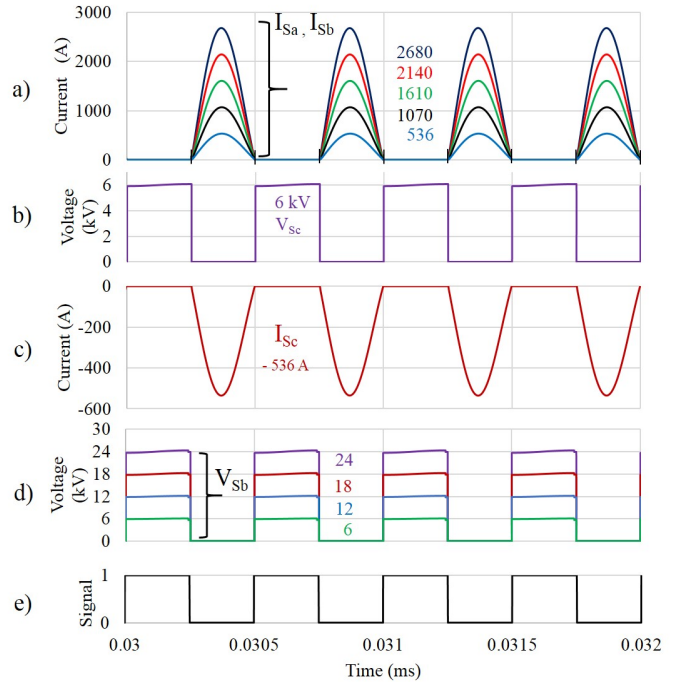Figure 12: Simulation waveforms of the forward mode operation.



Figure 13: IGBT and diode switches simulation waveforms of reverse mode operation: a) currents through cells A and B, b) stress voltage on cells C, c) charging current in series in cells A, and d) step voltage on cells B.

Waveforms of voltage, current, and power during reverse mode are shown in Figure 12. The voltage gain obtained by the simulation (0.204), is very close to the theoretical value of 0.2. The output voltage, current, and power of converter in reverse mode operation is also close to the theoretical values.

As illustrated in Figure 13(b), the voltage stress on the switch $S_b$ is 6 kV during discharge in series is equal to the $V_H/5$. The charging current in series is the same as through the IGBT switches (ISc= 536 A) as shown in Figure 13(c). One can see that the voltage on switches $S_b$ sequentially decreases in 6 kV steps as illustrated in Figure 13(d).

## 6 Conclusions

A new bidirectional DC-DC Marx converter is presented in this paper. Full mathematical analysis led to the design methodology to determine the component values and ratings including solid-state devices. The mathematical equations are validated by simulation. The simulation demonstrated the ability of the converter to interface a 6kV system with a 30kV system leading to a gain of 5. The gain can be increased for application to higher voltages by increasing the number of modules. Therefore, the converter is easily scaled up or down. The resonance between the inductors and capacitors are used to determine the switching frequency enabling soft switching to reduce the losses.

## References

[1]     S. M. Alagab, S. Tennakoon, and C. Gould, "Review of wind farm power collection schemes," In Power Engineering Conference (UPEC), *50th International Universities, pp. 1-5.* IEEE, 2015.

[2]     M. J. Carrizosa, A. Benchaib, P. Alou, and G. Damm, "DC transformer for DC/DC connection in HVDC network," *2013 15th Eur. Conf. Power Electron. Appl. EPE 2013*, 2013.

[3]     Z. Qin, Y. Shen, P. C. Loh, H. Wang, and F. Blaabjerg, "A Dual Active Bridge Converter with an Extended High-Efficiency Range by DC Blocking Capacitor Voltage Control," *IEEE Trans. Power Electron.*, vol. 8993, no. c, pp. 1–16, 2017.

[4]     T. Todor, P. Bauer, and J. A. Ferreira, "Bidirectional Modular Multilevel DC-DC Converter Control and Efficiency Improvements through Separate Module Control Method," pp. 2038–2043, 2013.

[5]     T. Lagier and P. Ladoux, "A comparison of insulated DC-DC converters for HVDC off-shore wind farms," *5th Int. Conf. Clean Electr. Power Renew. Energy Resour. Impact, ICCEP 2015*, pp. 33–39, 2015.

[6]     Z. Xing, X. Ruan, H. Xie, and X. Wang, "A modular bidirectional buck/boost dc/dc converter suitable for interconnecting HVDC grids," *2016 IEEE 8th Int. Power Electron. Motion Control Conf. IPEMC- ECCE Asia 2016*, pp. 3348–3354, 2016.

[7]     C. A. Pires Fernao, Foito D, "Bidirectional Boost/Buck Quadratic Converter for Distributed Generation Systems with Electrochemical Storage System," in *5th IET International Conference on Renewable Energy Research and Applications (ICRERA 2016)*, 2016, vol. 5, pp. 5–10.

[8]     D. Jovcic, "Bidirectional, high-power DC transformer," *IEEE Trans. Power Deliv.*, vol. 24, no. 4, pp. 2276–2283, 2009.

[9]     D. Jovcic, S. Member, L. Zhang, and S. Member, "LCL DC / DC Converter for DC Grids," vol. 28, no. 4, pp. 2071–2079, 2013.

[10]    M. G. Jahromi and G. Mirzaeva, "Design of a high power low losses DC-DC converter for mining applications," pp. 1–8, 2016.

[11]    S. K. Kolparambath, J. A. Suul, and ..., "Analysis of DC/DC converters in multiterminal HVDC systems for large offshore wind farms," ... *Power Energy (TAP ...,* pp. 415–420, 2015.

[12]    K. Filsoof and P. W. Lehn, "A bidirectional modular multilevel DC-DC converter of triangular structure," *IEEE Trans. Power Electron.*, vol. 30, no. 1, pp. 54–64, 2015.

[13]    P. Lakshmanan, J. Liang, and N. Jenkins, "Assessment of collection systems for HVDC connected offshore wind farms," *Electr. Power Syst. Res.*, vol. 129, pp. 75–82, Dec. 2015.

[14]    S. M. Alagab, S. B. Tennakoon, and C. A. Gould, "A Compact DC-DC Converter for Offshore Wind Farm Application," *Renew. Energy Power Qual. J.*, vol. 1, no. 15, pp. 529–533, 2017.

[15]    S. M. Alagab, S. B. Tennakoon, and C. A. Gould, "High Voltage Cascaded Step-Up DC-DC Marx Converter for Offshore Wind Energy Systems," *EPE 2017 - assigned jointly to Eur. Power Electron. Drives Assoc. Inst. Electr. Electron. Eng.*, no. Mmc, pp. 1–10, 2017.

[16]    ABB Switzerland Ltd., "Surge currents for IGBT diodes, Application Note 5SYA 2058-02," 2014.